

Optimized weighted non-local mean filter for enhanced denoising and improved quality of medical images

Aiswarya Senthilvel, Krishnaveni Marimuthu, Subashini Parthasarathy

Centre for Machine Learning and Intelligence, Department of Computer Science, Avinashilingam Institute for Home Science and Higher Education for Women, Coimbatore, India

Article Info

Article history:

Received Nov 13, 2024

Revised Jul 6, 2025

Accepted Jul 29, 2025

Keywords:

Blood smear images

Gradient degrading

Image denoising

Image quality enhancement

Medical image processing

ABSTRACT

Image quality is significantly influenced by noise, light, and artifacts, particularly in medical images where precision is essential for accurate diagnosis. Denoising is a significant pre-processing for enhancing the overall quality of images to enable efficient classification, feature extraction, and segmentation. Conventional denoising filters smooth out boundaries and lose texture because they are ineffective to process color images. To address these limitations, a weighted factor-based non-local means (WF+NLM) filter is proposed as an improvement over the non-local means (NLM) filter, with an additional weight factor based on pixel similarity. This addition reduces blurring while maintaining fine details, resulting in improved quality. The proposed filter performs effectively in blood smear images, with a peak signal-to-noise ratio (PSNR) of 39.6904, SSIM of 0.9551, and gradient SSIM of 0.9889. Statistical tests indicate that the WF+NLM filter improves image quality in terms of structure, gradients, and feature similarity. Statistical inference for a one-tailed paired t-test validates statistical significance with the highest t value of 9.323829 with p-value 0.00037 by the wavelet-based non-local moment mean (W-NMM) filter asserts higher image restoration quality.

This is an open access article under the [CC BY-SA](https://creativecommons.org/licenses/by-sa/4.0/) license.



Corresponding Author:

Aiswarya Senthilvel

Centre for Machine Learning and Intelligence, Department of Computer Science

Avinashilingam Institute for Home Science and Higher Education for Women

Coimbatore, Tamil Nadu, India

Email: 21phcsf007@avinuty.ac.in

1. INTRODUCTION

The peripheral blood smear images are essential for hematological examinations and provide significant health-related recommendations. This diagnostic process forms a thin blood coating on a glass slide, followed by dyed and evaluated under a microscope. The size, shape, and categorization of white blood cells (WBCs), red blood cells (RBCs), and platelets can provide essential information to medical professionals. These images are an important screening tool for diagnosing abnormalities such as anemia, infections, leukemias, and autoimmune disorders, thereby improving treatment and monitoring [1]. The clarity and brightness of blood smears are affected by different factors. Smear quality is determined by accurate thickness, equal spreading, and edge smoothness. Proper collection and extraction processes are necessary for preserving blood cell structure. Improper spreading will result in cell clustering, and a significant number of overlapping cells could make it difficult to detect the disease [2]. Images are acquired using different types of processes that create noise and distortions in the image. Removing noise from images is essential for a reliable diagnosis in medical image analysis. Gaussian, poisson, speckle, salt-and-pepper, and Rician noise are common in microscopic, computed tomography (CT), and magnetic resonance imaging

(MRI) images resulting from sensor imperfections, low-dose acquisition, and external factors during image capture. Denoising methods attempt to remove noise from images while retaining fine details. The challenges in medical imaging include retaining anatomical details, maintaining diagnostic integrity, handling modality-specific noise, and being compatible with tasks like segmentation and classification. Color image denoising is more challenging because of the complex spatial connections between the green, red, and blue channels. This technique aims to enhance the visual quality and color consistency by taking image texture, contrast, and illumination changes into consideration, and it also prevents unwanted impacts such as blurring. Traditional denoising methods, such as bilateral filtering, Gaussian, and median filters, are frequently used in the context of blood smear images but these methods are insufficient for color image denoising [3]–[7]. However, the non-local means (NLM) filter provides accurate interpretation by using dissimilarity measurements within particular regions to minimize noise in images [8]. The NLM filter was chosen because of its superior ability to preserve fine structural information by utilizing pixel similarity between non-local areas. The cellular structure in the image turns out to be smoothed, and the edges have been blurred when using the NLM denoising method. To overcome this challenge, this study proposes weighted factor-based non-local means (WF+NLM) enhancements in terms of intensity-spatial properties, effectively addressing issues such as color inconsistency and structural distortion.

The proposed denoising filter successfully reduces noise while maintaining the characteristics and general composition of the image. The paper has the following organizational structure: section 2 contains a summary of relevant research. A detailed explanation of the proposed WF+NLM filter is provided in section 3. The experimental results, obstacles, and benefits of the proposed denoising filter are provided in section 4, followed by a summary presented at the end of section 5.

2. RELATED WORK

Researchers have several conventional denoising approaches to enhance image quality. Guan *et al.* [9] suggested a hybrid image denoising approach that successfully resolves noise distortions by applying local thresholding to differentiate between salt-and-pepper and Gaussian pixels. The mean and median filtering algorithms were employed to denoise the affected pixels. The NLM filter was used because it successfully decreased Gaussian noise while maintaining fine features. Several modifications of the NLM approach have been developed to establish a suitable equilibrium between feature retention and noise reduction [10]. Li *et al.* [11] improved the NLM denoising algorithm by developing the adaptive nonlocal means (ANLM) technique, which modifies denoising intensity locally by employing a noise map. General non-local denoising model based on multi-kernel-induced measures (GNLKMIM) is an NLM model that was developed by Sun *et al.* [12] using multi-kernel-induced measures. While NLM-based algorithms excel at removing Gaussian noise, they have longer computation durations and higher resource utilization, which can result in obstructive artifacts and image blurring. Wang *et al.* [13] integrated fuzzy membership values with the NLM filter to develop the fuzzy decision non-local means (FDNLM) approach, which combines the benefits of fuzzy decision filters with edge preservation and noise reduction. Chen *et al.* [14] suggested a quaternion-based NLM filter for color image denoising, with applications focused mainly on medical data. NLM and the bidirectional filter improved non-local means (INLM) were integrated by Wang *et al.* [15] to improve NLM filters for color images. Liu and Zhang [16] proposed a denoising approach wavelet-based non-local moment mean (W-NMM) that combines wavelet transform with non-local moment mean (NMM) filtering. To improve noise reduction, the method starts with a wavelet-based soft technique and then adds NMM.

Deep learning advancements have enhanced the performance of image-denoising algorithms. A CNN-based denoising technique for low-dose “CT” was studied by Usui *et al.* [17] to determine its “dose-dependent properties”. An enhanced method known as denoising convolutional neural networks (DNCNN) was presented by Wang *et al.* [18]. It effectively denoises images by “sub-region processing and transfer learning”. The stacked convolutional autoencoder (SCAE) technique is used in Ahmed *et al.* [19] innovative denoising system for medical pictures. CNNs and autoencoders are combined in a medical image-denoising style developed by Sudha *et al.* [20]. Solovyeva and Abdullah [21] used a “dual autoencoder with separable convolutional layers for image denoising and deblurring”. Conventional denoising techniques, such as median filtering, frequently result in image blurring, which limits their applicability to finely detailed color images. Sahu *et al.* [22] proposed the “dual convolutional medical image-enhanced denoising network (DCMIEDN)” based on the DedeNet model. Deep learning-based denoising is limited by its reliance on big, high-quality datasets, inadequate numbers of real noisy images, unsupervised challenges in the absence of clean references, cost of computation, and weak preservation of fine diagnostic detail. To address these problems, this study proposes an improved filtering technique which utilizes an NLM filter with modified weight calculations for efficient color image denoising.

3. METHOD

3.1. Conventional non-local mean filter

The NLM filter was developed by Buades *et al.* [8] to minimize noise in the images by assigning weights based on the correlation between the central area patches and the neighboring patches in a specific search window. The color image is described as RGB_j , which consists of an array of weight (w) and height (h) in the format of $w \times h \times 3$. Each pixel intensity is described as a three-component vector of integers with values ranging from 0 to 255, where n indicates the method's three-color channels.

$$\underline{I}(d) = \frac{1}{Z(d)} \sum_{s \in \Omega} w(a, b) * I(d) \quad (1)$$

$$Z(d) = \sum_{s \in \Omega} w(a, b) \quad (2)$$

$$w(a, b) \exp\left(-\frac{(\|f(a) - f(b)\|^2)}{2h^2}\right) \quad (3)$$

The NLM filter is expressed mathematically using (1) to (3). In (1) computes the filtered pixel intensity $I(d)$ at location d using a weighted average of intensities in the neighborhood Ω . In (2) specifies $Z(d)$, a normalization factor that ensures the weights are scaled properly. In (3) calculates the weight $w(a, b)$ as an exponential function of the squared Euclidean distance between feature vectors $f(a)$ and $f(b)$ divided by $2h^2$, where h is the filtering parameter. The weight decreases significantly as the dissimilarity between patches increases. This approach effectively denoises by comparing the similarities between a target patch and nearby patches in a search window. However, the computational cost of processing multi-channel (color) images remains significant due to their higher dimensionality. Furthermore, illumination variations and smooth color gradients frequently result in incorrect weight estimation, resulting in poor denoising performance. Additionally, the NLM filter is unable to handle spatially non-uniform noise, which can occasionally result in the removal of crucial structural elements like cell borders. Figure 1 illustrates the NLM filter's denoising capabilities on a blood smear image. Figure 1(a) exhibits the original image, whereas Figure 1(b) demonstrates effective noise removal; however, the structure and boundaries become smoothed.

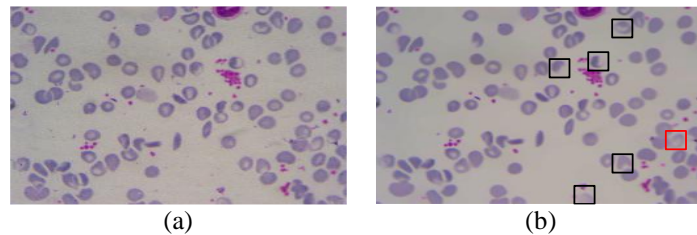


Figure 1. NLM filter performance on blood smear image; (a) source image and (b) denoised image

3.2. Proposed weight factor non-local mean filter

The proposed WF+NLM filter addresses the shortcomings of traditional NLM denoising techniques by including an additional weight factor that captures spatial and intensity variations. The weight factor $w1(p, q)$ is used to improve the similarity measurement by accounting for pixel intensity variance within local patches, as shown in (4). This weight term is computed by taking the squared Euclidean distance between the intensities of two patches: the central patch ($I(p, q)$) and the adjacent patch ($I(m, n)$) and it is represented mathematically by (5). The squared intensity difference between two image patches, represented as $\|I(m, n) - I(p, q)\|^2$, is calculated by adding the squared intensity differences between corresponding pixels (i, j) in patches P and Q with centers at (m, n) and (p, q) , respectively. The lower the value, the more similar the patches are in intensity; the higher the value, the more dissimilar. The $F(\cdot)$ function converts squared Euclidean distance to a weighting metric that prioritizes pixel intensity changes. The extra component is combined with the standard NLM weight function to form a hybrid weight, as shown in (6).

$$w1(p, q) = F(\|I(m, n) - I(p, q)\|^2) \quad (4)$$

$$\|I(m, n) - I(p, q)\|^2 = \sum_{i, j} [I_P(i, j) - I_Q(i, j)]^2 \quad (5)$$

$$w(a, b) = \exp\left(-\frac{(\|f(a) - f(b)\|^2)}{2h^2}\right) w1(p, q) \quad (6)$$

The weighted composite method combines spatial proximity and photometric dissimilarity. The exponential term calculates patch similarity using a Gaussian kernel, with $w1(p,q)$ determining the weight based on pixel intensity gradients. This method is more effective at noise reduction and edge preservation, especially for images with strong boundaries or varying lighting. With the weight factor $w1$ for intensity similarity and the exponential factor for spatial weight, the proposed WF+NLM filter illustrates the significance of pixels adjacent to each other and having close spatial weights comparable in intensity. Algorithm 1 explains the entire denoising procedure step by step, from patch extraction to weight computation and normalization. Denoising was tested on colored images with a 3×3 patch size and search window size. These small sizes maintain computational efficiency while preserving structural details. The filtering parameter h was configured to 0.1 because it generates beneficial smoothing without excessive blurring while removing noise. The proposed method is not dependent on any specific dataset but is tested on images with varying lighting conditions to ensure generalizability. Selecting $\sigma=0.1$ aligns with previous research indicating that Gaussian-like noise patterns perform best when suppressed while retaining texture and edges. Experimentation with color images under changing illumination confirms the method's robustness and efficacy in maintaining sharpness and reducing noise.

Algorithm 1: Proposed WF+NLM filter for color image

Input: Image I , patch Size =3, Search window size =3, Filter parameter $h=0.1$

For each pixel (a, b) in image I :

Define a patch P centered at (a, b) with size patch Size

Initialize total Weight = 0

Initial Weighted Sum = 0

For each pixel (m, n) in the search window around (a, b) :

Defining a patch Q centered at (m, n) with size patch Size

Use (3) to Calculate feature similarity $f(a)$ and $f(b)$

Calculate squared Euclidean distance $\|f(a) - f(b)\|^2$

Use (4) to Calculate $w1(p, q)$

Using (6) to Calculate $w(a, b)$ using $w1$ and feature similarity:

*Update weightedSum $+= w * I(m, n)$*

Update totalWeight $+= w$

Use equation (1) to Calculate normalized denoised intensity at (a, b) :

Output: Denoised image I

4. EXPERIMENTAL ANALYSIS

This study compares the WF+NLM filter's performance to existing methods in denoising color medical images, using both qualitative and quantitative analysis.

4.1. Dataset description

This study makes use of several types of different medical image databases. Images of sickle cell peripheral blood smears were obtained from the ErythrocytesIDB1 database [23] with a Leica microscope at 100x magnification and resized to 256×256 pixels for analysis. Additional images for testing the WF+NLM filter were obtained from Kaggle, such as the BreakHis database [24], which contains breast cancer histopathological images of 700×460 pixels and 400x magnification, frequently with Gaussian noise. Body cavity fluid cytology images [25] 256×192 pixels, 40x magnification have been affected by Gaussian and speckle noise. Grayscale images of the Breast Ultrasound Dataset [26] (449×598 pixels) and the Large COVID-19 CT scan slice dataset [27] 512×512 pixels, both with Gaussian and Poisson noise, were also used to evaluate denoising.

4.2. Quality assessment techniques

The quantitative evaluation was performed to evaluate the proposed denoising filter with existing methods. This evaluation consisted of metrics such as mean squared error (MSE), peak signal-to-noise ratio (PSNR), and normalized mean square error (NMSE), which are denoted by (7) to (9), respectively. Visual examination and analysis of structural variations were used to determine the overall similarity between the two images. The multi-scale structure similarity index method (MS-SSIM), gradient-based structure similarity index method (GSSIM), and feature similarity index matrix (FSIM) were used in this analysis of the structure similarity of the denoised images. In (10) to (13) [28]–[31] were applied to examine the image boundary features and structure, providing essential information and distinctive features of the denoised images.

$$PSNR = \frac{3 \cdot 255^2}{\frac{1}{XY} \sum_{p=0}^X \sum_{q=1}^Y [\hat{a}(p,q) - a(p,q)]^2} \tag{7}$$

$$MSE = \frac{1}{3XY} \sum_{j=0}^X \sum_{i=1}^Y [\hat{a}(p,q) - a(p,q)]^2 \tag{8}$$

$$NMSE = \frac{\sum_{p=0}^X \sum_{q=1}^Y [\hat{a}(p,q) - a(p,q)]^2}{\sum_{p=0}^X \sum_{q=1}^Y [a(p,q)]^2} \tag{9}$$

$$SSIM(i,j) = \frac{(2\mu_i\mu_j + C_1)(2\sigma_{ij} + C_2)}{(\mu_i^2 + \mu_j^2 + C_1)(\sigma_i^2 + \sigma_j^2 + C_2)} \tag{10}$$

$$MS - SSIM(i,j) = l_x(i,j) \cdot \prod_{x=1}^X C_x(i,j) S_x(i,j) \tag{11}$$

$$GSSIM(i,j) = \frac{(2\mu_i\mu_j + C_1)(2\sigma_{ij} + C_2)}{(\mu_i^2 + \mu_j^2 + C_1)(\sigma_i^2 + \sigma_j^2 + C_2)} \tag{12}$$


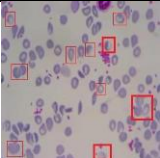
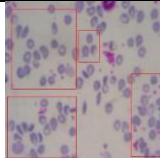

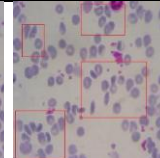
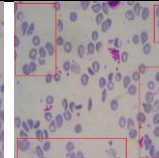
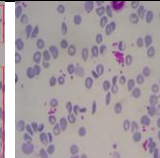
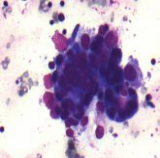
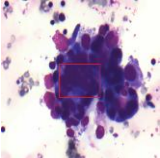
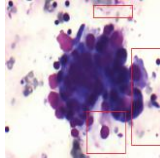
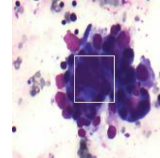
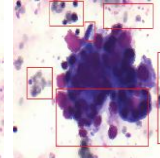
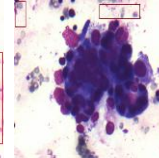
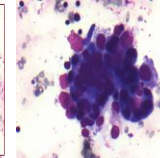
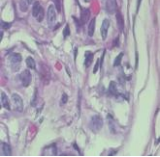
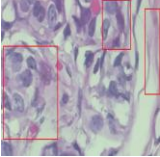
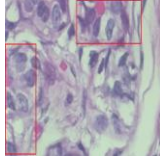
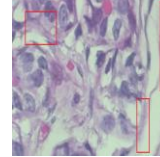
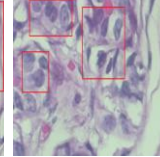
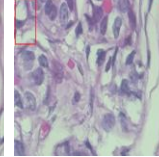
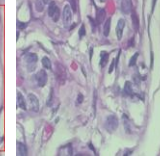
$$FSIM(S_M(a)) = [S_{PC}(a)]^\alpha \cdot [S_G(a)]^\beta \tag{13}$$

The significant components of an image analysis process are detailed by (7) to (13). In these equations, the variables (i,j) define the positions of an image, $a(p,q)$ represent the original images, and $\hat{a}(p,q)$ represent the filtered image. Besides, σ_i^2 and σ_j^2 denote the variances of i and j and the correlation coefficient of their covariance. Constants C_1 and C_2 are essential for reducing computational uncertainty once the denominator approaches zero. The two images are compared and determined by i and j using gradient-based distinction comparison maps. MS-SSIM denotes the original image as l and the scaling aspect as M . For the e th scale $C_i(i,j)$ and $S_i(i,j)$ represents the contrast and structure findings at different levels. The notation $l_p(i,j)$ represents the brightness correlation in scale M . The FSIM method identifies peculiar phase congruency (PC) and gradient magnitude (G) requirements. The structural similarity index is employed in the range $[0, 1]$, with higher standards indicating more significant image quality. The proposed approach reduces aberrations in blood smear color images, resulting in better outcomes. The WF+NLM denoising method is examined in decreasing noise and obtaining cell structure and color features. Using established techniques like NLM [8], ANLM [11], FDNLM [13], INLM [15], and W-NMM [16], the algorithm efficiency is evaluated.

4.3. Qualitative analysis

The qualitative performance of various denoising techniques was tested on three types of medical images blood smears, cytology, and histopathology—using six filtering techniques: NLM, ANLM, FDNLM, INLM, WNMM, and the WF+NLM filter proposed in this paper. The denoised images are presented in Table 1. The WF+NLM filter outperformed the others as a denoiser, effectively removing noise while preserving important cellular architecture and color integrity.

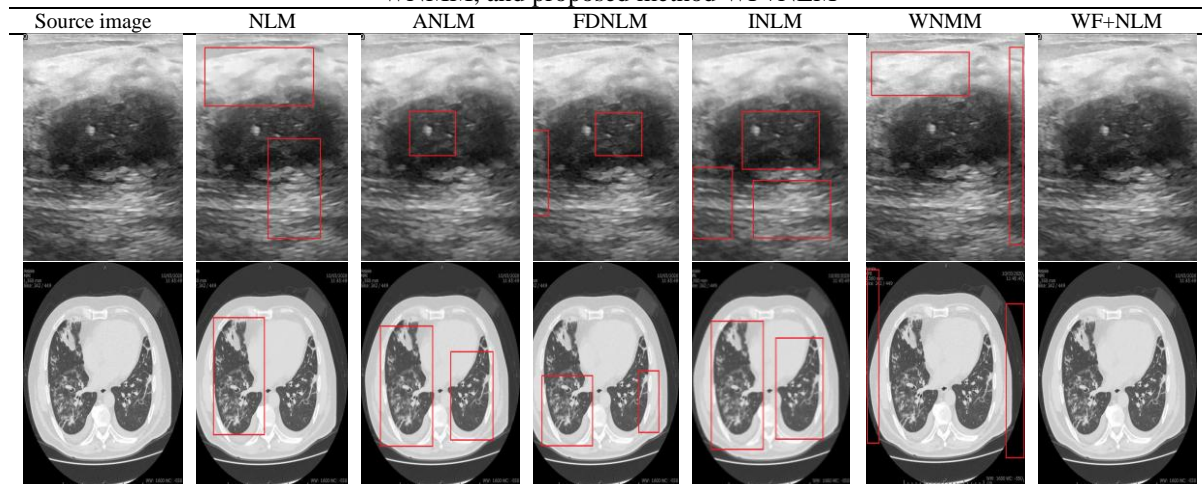
Table 1. Denoising comparison of different denoising methods on cytology and histopathology with NLM, ANLM, FDNLM, INLM, WNMM, and proposed method

Source image	NLM	ANLM	FDNLM	INLM	WNMM	WF+NLM
						
						
						

However, only the WF+NLM filter consistently maintained clear cellular edges and accurate chromatic representation. The NLM filter reduced noise sparsely, but it sacrificed edge sharpness and chromatic details. ANLM reduced speckle noise but increased color distribution and over-smoothing. FDNLM improved color accuracy but resulted in blurred cellular edges. In contrast, WNMM was unable to eliminate any remaining noise and resulted in membrane distortion, while INLM produced excessive structural smoothing. WF+NLM, on the other hand, successfully restored erythrocyte morphology while preserving membrane definition and cell coloration. Traditional denoising techniques were tested in the second row using cytology images with complex cellular morphology and fine granularity. NLM reduced noise but improved cytoplasmic texture. ANLM maintained spatial information at the expense of color integrity. FDNLM balanced noise reduction and structure preservation, but micron-scale features were blurred. INLM softened the edges, while WNMM added the remaining patchy noise. The WF+NLM filter, on the other hand, successfully combined spatial and intensity information, improving subcellular detail and membrane definition, thereby increasing nucleocytoplasmic contrast without causing artifacts.

In the third row, histopathology images revealed intricate tissue structures and stain heterogeneity, necessitating advanced denoising. Conventional filters such as NLM and FDNLM removed background noise while uniformly distributing stain intensities. ANLM introduced uneven artifacts, whereas INLM excessively blurred tissue boundaries. WNMM was ineffective in noise reduction. Conversely, the WF+NLM filter performed better by retaining significant stain gradients, improving tissue interface delineation, and establishing structural preservation across both homogeneous stromal and heterogeneous glandular areas without compromising diagnostic accuracy. A qualitative examination of the denoised grayscale images from Table 2 demonstrates that the WF+NLM filter proposed in the paper produces visually superior results than conventional approaches. WF+NLM can effectively suppress both Gaussian and Poisson noise in ultrasound and CT scan images while preserving essential anatomical structures and edge definitions. Conventional filters, such as NLM, ANLM, and INLM, smooth fine details while leaving residual noise artifacts behind. FDNLM retains structure moderately but at the expense of clarity, whereas WNMM does not effectively mask noise. The WF+NLM filter preserves textural detail and tissue boundary coherence in grayscale medical imaging, enhancing visual interpretability and diagnostic value.

Table 2. Comparison of denoising methods on ultrasound and CT scan with NLM, ANLM, FDNLM, INLM, WNMM, and proposed method WF+NLM



4.4. Quantitative analysis

The quantitative assessment across three microscopy modalities reveals that the proposed WF+NLM filter has a better denoising ability. For blood smear images, see Table 3, WF+NLM achieved a PSNR of 39.69 dB, which was more than 7 dB higher than conventional NLM (32.46 dB) and ANLM (32.04 dB). It reduced MSE to 4.74 and NMSE to 0.00018, while NLM increased to 13.02 and 0.00051, respectively. Structural similarity measures increased significantly, with SSIM at 0.9551, MS-SSIM at 0.9422, and GSSIM at 0.9889, indicating improved edge and texture preservation. In images of cavity fluid cytology, see Table 4, WF+NLM produced PSNR of 41.68 dB, which was higher than NLM's 38.46 dB, with MSE down to 20.99 from 23.91 and NMSE down to 0.00051 from 0.00058. The proposed WF+NLM filter has better denoising capability, as evidenced by the quantitative assessment across three microscopy modalities.

WF+NLM achieved a PSNR of 39.69 dB in blood smear images, see Table 3, more than 7 dB higher than conventional NLM (32.46 dB) and ANLM (32.04 dB).

Table 3. Denoising performance comparison of blood smear images with NLM, ANLM, FDNLM, INLM, WNMM, and proposed filter WF+NLM

Filter methods	PSNR	MSE	NMSE	SSIM	MS-SSIM	GSSIM	FSIM
NLM [8]	32.4609	13.0162	0.00051	0.9228	0.8903	0.9324	0.9074
ANLM [11]	32.0414	30.5319	0.0012	0.8847	0.8192	0.7444	0.8096
FDNLM [13]	32.7631	14.8113	0.00059	0.9214	0.8884	0.9049	0.8982
INLM [15]	31.0639	38.9835	0.00155	0.8652	0.7966	0.6924	0.8118
WNMM [16]	22.0186	480.696	0.01916	0.4155	0.0351	-0.0102	0.4140
WF+NLM	39.6904	4.7432	0.00018	0.9551	0.9422	0.9889	0.9430

Table 4. Denoising performance comparison for cavity fluid cytology images with NLM, ANLM, FDNLM, INLM, WNMM, and proposed filter WF+NLM

Existing methods	PSNR	MSE	NMSE	SSIM	MS-SSIM	GSSIM	FSIM
NLM [8]	37.8133	10.3586	0.00034	0.9407	0.9060	0.9318	0.9167
ANLM [11]	38.0245	11.6255	0.00038	0.9462	0.9206	0.9231	0.9270
FDNLM [13]	38.2108	9.9862	0.00033	0.9505	0.9322	0.9565	0.9434
INLM [15]	36.2182	17.0770	0.00056	0.9264	0.8862	0.8555	0.9009
WNMM [16]	22.7609	390.2984	0.0129	0.4979	0.1007	0.1377	0.4979
WF+NLM	41.0948	6.3425	0.00034	0.9682	0.9548	0.9728	0.9583

In contrast to NLM's 13.02 and 0.00051, respectively, it reduced MSE to 4.74 and NMSE to 0.00018. The structural similarity index scores were significantly higher, with SSIM 0.9551, MS-SSIM 0.9422, and GSSIM 0.9889, indicating better edge and texture preservation. Table 4 demonstrates that the WF+NLM technique denoised cavity fluid cytology images more effectively than traditional filters, with a maximum PSNR of 41.09 dB, a reduced MSE of 6.34, and an increased structural similarity index of 0.9682. The findings of histopathological pictures displayed in Table 5 indicate that the WF+NLM achieved a PSNR of 41.68 dB, exceeding NLM's 38.46 dB, with MSE decreasing to 20.99 from 23.91 and NMSE decreasing to 0.00051 from 0.00058.

Table 5. Denoising performance comparison for histopathology images with NLM, ANLM, FDNLM, INLM, WNMM, and proposed filter WF+NLM

Existing methods	PSNR	MSE	NMSE	SSIM	MS-SSIM	GSSIM	FSIM
NLM [8]	38.4627	23.9072	0.00058	0.9575	0.9325	0.9906	0.9542
ANLM [11]	34.2336	35.2182	0.00086	0.9443	0.9145	0.9675	0.9281
FDNLM [13]	36.2685	27.5218	0.00067	0.9443	0.9475	0.9853	0.9578
INLM [15]	29.7679	84.5754	0.00208	0.9143	0.8719	0.8986	0.9024
WNMM [16]	15.3447	2117.776	0.0521	0.3960	0.0414	0.0363	0.3959
WF+NLM	41.6788	20.9883	0.00051	0.9832	0.9357	0.9954	0.9816

Tables 6 and 7 show quantitative evaluations of grayscale breast cancer ultrasound and COVID-19 CT images, demonstrating the WF+NLM filter's more accurate denoising performance. In ultrasound images, WF+NLM obtained a maximum PSNR of 42.97 dB, compared to 40.87 dB for NLM and 40.88 dB for FDNLM, minimizing MSE to 3.27 and NMSE to 0.00018. The structural similarity indices are SSIM 0.9787, MS-SSIM 0.9658, and GSSIM 0.9709, indicating superior texture and boundary preservation. In grayscale COVID-19 CT images, WF+NLM achieved 40.87 dB PSNR, exceeding NLM's 39.41 dB and FDNLM's 36.39 dB, with an MSE of 5.32 and an NMSE of 0.00025. SSIM improved to 0.9515, MS-SSIM to 0.9333, and GSSIM to 0.9915, ensuring effective noise removal while preserving important anatomical details. Compared to traditional methods, WF+NLM provided reliable edge preservation, noise reduction, and structural robustness.

Table 6. Denoising performance comparison of breast cancer ultrasound images with NLM, ANLM, FDNLM, INLM, WNMM and proposed filter WF+NLM

Filter methods	PSNR	MSE	NMSE	SSIM	MS-SSIM	GSSIM	FSIM
NLM [8]	40.8763	5.3271	0.0003	0.9658	0.9421	0.9519	0.9550
ANLM [11]	37.4221	11.7724	0.00066	0.9410	0.9020	0.9452	0.9005
FDNLM [13]	40.8809	5.3291	0.00030	0.9787	0.9590	0.9771	0.9595
INLM [15]	33.7214	27.6017	0.00155	0.8894	0.8203	0.8613	0.8343
WNMM [16]	20.2277	617.0371	0.03475	0.2687	0.0215	0.0826	0.2685
WF+NLM	42.9726	3.2795	0.00018	0.9787	0.9658	0.9709	0.9695

Table 7. Denoising performance comparison of COVID-19 CT scan images with NLM, ANLM, FDNLM, INLM, WNMM and proposed filter WF+NLM

Filter methods	PSNR	MSE	NMSE	SSIM	MS-SSIM	GSSIM	FSIM
NLM [8]	39.4084	7.4357	0.00035	0.9413	0.9185	0.9889	0.9295
ANLM [11]	34.1524	24.9941	0.00118	0.8825	0.8436	0.9549	0.8424
FDNLM [13]	36.3922	14.9251	0.00070	0.9207	0.8996	0.9781	0.9024
INLM [15]	28.0071	102.889	0.00489	0.8085	0.7409	0.8185	0.7549
WNMM [16]	15.8933	1673.96	0.07956	0.3935	0.0608	0.0055	0.3934
WF+NLM	40.8687	5.3235	0.00025	0.9515	0.9333	0.9915	0.9411

4.5. Statistical evaluation of denoising performance

The performance comparison of the proposed WF+NLM filter and other denoising methods NLM, ANLM, FDNLM, INLM, and WNMM is statistically evaluated through four image quality measures SSIM, MS-SSIM, GSIM, and FSIM in Table 8. A one-tailed paired t-test was employed to compare the performance improvement of the proposed denoising filters over the conventional methods assuming normality in the differences employing (14). Statistical significance was ascertained at 95% confidence ($\alpha=0.05$). Results indicate that all the proposed filters performed better than conventional methods regarding SSIM. In the statistical calculation, D is the difference between any two observations, N is the number of paired observations, $\sum D$ is the sum of all the differences, and $\sum D^2$ is the sum of the square of each difference. For instance, the t-value for NLM filter was 5.038318 while the p-value was 0.00365, which represents a notable enhancement. Similarly, the ANLM filter showed a t-value of 5.007947 and a p-value of 0.00372, confirming its efficiency.

$$t = \frac{(\sum D)/N}{\sqrt{\frac{\sum D^2 - \frac{(\sum D)^2}{N}}{(N-1)(N)}}} \quad (14)$$

Table 8. Statistical significance analysis of the proposed WF+NLM filter compared to traditional methods

Metrics	NLM	ANLM	FDNLM	INLM	WNMM
SSIM	5.038318	5.007947	4.896924	5.714129	9.323829
MS-SSIM	5.087125	4.95939	3.389371	6.244257	52.007462
GSIM	3.108303	2.268464	2.8102	4.305715	29.942231
FSIM	4.492921	4.329255	4.181874	5.192905	14.239511

The FDNLM filter yielded a t-value of 4.896924 with a p-value of 0.00403, confirming the effectiveness of the proposed filters. The INLM filter reported a t-value of 5.714129 and a p-value of 0.00232, indicating a significant influence. The proposed WF+NLM filter has a higher time complexity than NLM and ANLM because it has more processing steps. However, compared to INLM, WNMM, and FDNLM filters, it is computationally more efficient. The model was trained on a high-performance setup using a Tesla V100 PCIe GPU and CUDA 12.5, with processing times of 12.3 s for NLM, 13.1 s for ANLM, 18.7 s for WF+NLM, 20.58 s for INLM, 26.1 s for WNMM, and 25.3 s for FDNLM. The WNMM filter had the highest statistical significance t-value of 9.323829, and p-value of 0.00037, demonstrating the proposed method's excellent performance. These findings support the effectiveness of the proposed denoising techniques in significantly improving image quality when compared to conventional methods.

The integrated NLM filter, which combines spatial and intensity weight elements, enables improved denoising performance. The proposed weight factor $w_1(p, q)$ prioritizes preserving pixel intensity changes, significantly facilitating decreased noise while preserving visual details, especially in regions with sharp intensity transitions. Employing the squared Euclidean distance for pixel intensity similarity, the proposed

weight calculation approach reliably enhances denoising across different images. Multiplying spatial weight $w(a,b)$ by intensity weight $w_1(p,q)$ magnifies the effect of similar patches, accentuating edges, decreasing blurring, and improving overall image quality. The outcomes of evaluating color and grayscale images demonstrate that NLM, ANLM, and FDNLM techniques effectively reduce noise. However, they have restrictions in maintaining cell structure and borders in cytology, histopathology, ultrasound, and CT scan images. The WNMM approach must provide more outcomes for color and grayscale images, while INLM filters perform efficiently for histopathology images. The proposed WF+NLM denoising filter performs more effectively than conventional algorithms on different types of images.

5. CONCLUSION

The WF+NLM filter outperforms traditional denoising techniques, particularly color image denoising, by adding an extra weight component to effectively manage spatial variation and pixel value variation. The filter makes significant improvements in both color and grayscale medical images, with color image PSNR values ranging from 2 to 6 dB and structural similarity (SSIM) improving by 2 to 4 points. For grayscale images, PSNR scores rise by 2 dB, while SSIM increases by 2 to 3 points. These findings demonstrate the WF+NLM filter's superiority in preserving critical image features, making it an effective tool for image segmentation and classification. Statistical analysis also validates its performance, with the WF+NLM filter outperforming traditional methods, as evidenced by significant SSIM, MS-SSIM, GSIM, and FSIM improvements. The WNMM filter had the highest statistical significance, with a t-value of 9.323829 and a p-value of 0.00037. Future work will focus on increasing the computational efficiency of this method in order to further reduce processing time.

FUNDING INFORMATION

The authors extend their gratitude to the Centre for Machine Learning and Intelligence (CMLI), funded by the Department of Science and Technology DST/CURIE-AI/04/2020-PHASE-II(G), India, for providing facilities to support this research.

AUTHOR CONTRIBUTIONS STATEMENT

This journal uses the Contributor Roles Taxonomy (CRediT) to recognize individual author contributions, reduce authorship disputes, and facilitate collaboration.

Name of Author	C	M	So	Va	Fo	I	R	D	O	E	Vi	Su	P	Fu
Aiswarya Senthilvel	✓	✓	✓	✓	✓	✓		✓	✓	✓	✓		✓	
Krishnaveni	✓	✓		✓		✓		✓		✓	✓	✓		✓
Marimuthu														
Subashini	✓			✓			✓			✓	✓			✓
Parthasarathy														

C : **C**onceptualization

M : **M**ethodology

So : **S**oftware

Va : **V**alidation

Fo : **F**ormal analysis

I : **I**nvestigation

R : **R**esources

D : **D**ata Curation

O : Writing - **O**riginal Draft

E : Writing - Review & **E**ditting

Vi : **V**isualization

Su : **S**upervision

P : **P**roject administration

Fu : **F**unding acquisition

CONFLICT OF INTEREST STATEMENT

Authors state no conflict of interest.





DATA AVAILABILITY

The data that support the findings of this study are openly available in [ErythrocytesIDB] at <http://erythrocytesidb.uib.es/>. reference number [23] and [Kaggle] at <https://www.kaggle.com/datasets/> references number [24]–[26].





REFERENCES

- [1] A. S. Adewoyin and B. Nwogoh, "Peripheral blood film - a review," *Annals of Ibadan Postgraduate Medicine*, vol. 12, no. 2, pp. 71–9, 2014.
- [2] W. M. F. Amaris, C. Martinez, L. J. Cortés-Cortés, and D. R. Suárez, "Image features for quality analysis of thick blood smears employed in malaria diagnosis," *Malaria Journal*, vol. 21, no. 1, pp. 1–12, 2022, doi: 10.1186/s12936-022-04064-2.
- [3] T. P. Deepa and A. N. Rao, "A Study on Denoising of Poisson Noise in Pap Smear Microscopic Image," *Indian Journal of Science and Technology*, vol. 9, no. 45, pp. 1–10, 2016, doi: 10.17485/ijst/2016/v9i45/96623.
- [4] A. K. Boyat and B. K. Joshi, "A Review Paper: Noise Models in Digital Image Processing," *Signal & Image Processing: An International Journal*, vol. 6, no. 2, pp. 63–75, 2015, doi: 10.5121/sipij.2015.6206.
- [5] L. Fan, F. Zhang, H. Fan, and C. Zhang, "Brief review of image denoising techniques," *Visual Computing for Industry, Biomedicine, and Art*, vol. 2, no. 1, 2019, doi: 10.1186/s42492-019-0016-7.
- [6] I. Pitas and A. N. Venetsanopoulos, *Nonlinear Digital Filters: Principles and Applications*. Boston, MA: Springer US, 1990, doi: 10.1007/978-1-4757-6017-0.
- [7] C. Tomasi and R. Manduchi, "Bilateral filtering for gray and color images," in *Proceedings of the IEEE International Conference on Computer Vision*, 1998, pp. 839–846, doi: 10.1109/iccv.1998.710815.
- [8] A. Buades, B. Coll, and J. M. Morel, "A non-local algorithm for image denoising," in *Proceedings - 2005 IEEE Computer Society Conference on Computer Vision and Pattern Recognition, CVPR 2005*, 2005, pp. 60–65, doi: 10.1109/CVPR.2005.38.
- [9] X. P. Guan, L. X. Zhao, and Y. G. Tang, "Mixed filter for image denoising," *Journal of Image and Graphics*, vol. 10, pp. 332–337, 2005.
- [10] Y. Zheng, B. Jeon, J. Zhang, and Y. Chen, "Adaptively determining regularisation parameters in non-local total variation regularisation for image denoising," *Electronics Letters*, vol. 51, no. 2, pp. 144–145, 2015, doi: 10.1049/el.2014.3494.
- [11] Z. Li *et al.*, "Adaptive nonlocal means filtering based on local noise level for CT denoising," *Medical Physics*, vol. 41, no. 1, pp. 1–16, 2014, doi: 10.1118/1.4851635.
- [12] Z. Sun, S. Chen, and L. Qiao, "A general non-local denoising model using multi-kernel-induced measures," *Pattern Recognition*, vol. 47, no. 4, pp. 1751–1763, 2014, doi: 10.1016/j.patcog.2013.11.003.
- [13] G. Wang, H. Zhu, and Y. Wang, "Fuzzy decision filter for color images denoising," *Optik*, vol. 126, no. 20, pp. 2428–2432, 2015, doi: 10.1016/j.ijleo.2015.06.005.
- [14] B. Chen, Q. Liu, X. Sun, X. Li, and H. Shu, "Removing Gaussian noise for colour images by quaternion representation and optimisation of weights in non-local means filter," *IET Image Processing*, vol. 8, no. 10, pp. 591–600, 2014, doi: 10.1049/iet-ipr.2013.0521.
- [15] G. Wang, Y. Liu, W. Xiong, and Y. Li, "An improved non-local means filter for color image denoising," *Optik*, vol. 173, pp. 157–173, 2018, doi: 10.1016/j.ijleo.2018.08.013.
- [16] C. Liu and L. Zhang, "A Novel Denoising Algorithm Based on Wavelet and Non-Local Moment Mean Filtering," *Electronics (Switzerland)*, vol. 12, no. 6, pp. 1–13, 2023, doi: 10.3390/electronics12061461.
- [17] K. Usui, K. Ogawa, M. Goto, Y. Sakano, S. Kyougoku, and H. Daida, "Quantitative evaluation of deep convolutional neural network-based image denoising for low-dose computed tomography," *Visual Computing for Industry, Biomedicine, and Art*, vol. 4, no. 1, pp. 1–9, 2021, doi: 10.1186/s42492-021-00087-9.
- [18] J. Wang, Y. Tang, J. Zhang, M. Yue, and X. Feng, "Convolutional neural network-based image denoising for synchronous measurement of temperature and deformation at elevated temperature," *Optik*, vol. 241, 2021, doi: 10.1016/j.ijleo.2021.166977.
- [19] A. S. Ahmed, W. H. El-Beahdy, and A. A. A. Youssif, "Medical image denoising system based on stacked convolutional autoencoder for enhancing 2-dimensional gel electrophoresis noise reduction," *Biomedical Signal Processing and Control*, vol. 69, pp. 1–8, 2021, doi: 10.1016/j.bspc.2021.102842.
- [20] V. Sudha, K. Kalyanasundaram, R. C. S. Abishek, and R. Raja, "A Medical Image Enhancement to Denoise Poisson Noises Using Neural Network and Autoencoders," in *Lecture Notes in Networks and Systems*, vol. 436, 2022, pp. 717–725, doi: 10.1007/978-981-19-1012-8_50.
- [21] E. Solovyeva and A. Abdullah, "Dual Autoencoder Network with Separable Convolutional Layers for Denoising and Deblurring Images," *Journal of Imaging*, vol. 8, no. 9, pp. 1–22, 2022, doi: 10.3390/jimaging8090250.
- [22] A. Sahu, K. P. S. Rana, and V. Kumar, "An application of deep dual convolutional neural network for enhanced medical image denoising," *Medical and Biological Engineering and Computing*, vol. 61, no. 5, pp. 991–1004, 2023, doi: 10.1007/s11517-022-02731-9.
- [23] P. M. Fernández *et al.*, "ErythrocytesIDB (Version 2, October 2017)," [www.uib.es](http://erythrocytesidb.uib.es/). [Online]. Available: <http://erythrocytesidb.uib.es/>. (accessed: Jul. 06, 2025).
- [24] K. Muzaki, "BrecaKHis 400X: Breast cancer images on histopathology slides," Kaggle.com. [Online]. Available: <https://www.kaggle.com/datasets/forderation/breakhis-400x>. (accessed: Jul. 6, 2025).
- [25] P. Sanyal, "Body cavity fluid cytology images: Benign and malignant cell clusters from body cavity effusions," Kaggle.com. [Online]. Available: <https://www.kaggle.com/datasets/cmacus/body-cavity-fluid-cytology-images>. (accessed: Jul. 06, 2025).
- [26] A. Shah, "Breast Ultrasound Images Dataset: Breast ultrasound images for classification, detection & segmentation," Kaggle.com. [Online]. Available: <https://www.kaggle.com/datasets/aryashah2k/breast-ultrasound-images-dataset>. (accessed: Jul. 06, 2025).
- [27] M. Maftouni, "Large COVID-19 CT scan slice dataset: Curated COVID-19 CT scan dataset from 7 public datasets," Kaggle.com. [Online]. Available: <https://www.kaggle.com/datasets/maedemaftouni/large-covid19-ct-slice-dataset>. (accessed: Jul. 06, 2025).
- [28] U. Sara, M. Akter, and M. S. Uddin, "Image Quality Assessment through FSIM, SSIM, MSE and PSNR—A Comparative Study," *Journal of Computer and Communications*, vol. 7, no. 3, pp. 8–18, 2019, doi: 10.4236/jcc.2019.73002.
- [29] C. Li and A. C. Bovik, "Three-component weighted structural similarity index," *Image Quality and System Performance VI*, vol. 7242, pp. 252–260, 2009, doi: 10.1117/12.811821.
- [30] Z. Wang, E. P. Simoncelli, and A. C. Bovik, "Multi-scale structural similarity for image quality assessment," in *Conference Record of the Asilomar Conference on Signals, Systems and Computers*, 2003, pp. 1398–1402. doi: 10.1109/acssc.2003.1292216.
- [31] A. C. Brooks, X. Zhao, and T. N. Pappas, "Structural similarity quality metrics in a coding context: Exploring the space of realistic distortions," *IEEE Transactions on Image Processing*, vol. 17, no. 8, pp. 1261–1273, 2008, doi: 10.1109/TIP.2008.926161.





BIOGRAPHIES OF AUTHORS

Aiswarya Senthilvel     is a research scholar in the Department of Computer Science, at Avinashilingam Institute for Home Science and Higher Education for Women, Coimbatore, India. Her area of interest includes medical image processing, optimization technique, computer vision, artificial intelligence, and deep learning. She can be contacted at email: 21phcsf007@avinuty.ac.in.



Krishnaveni Marimuthu     is an Assistant Professor (SG) of the Department of Computer Science, Avinashilingam University for Women, Coimbatore, Tamil Nadu, India. She holds the position of being in charge of the AAI Startup program within the Centre for Machine Learning and Intelligence. She has published 4 books, 7 book chapters and 90 research papers in both national and international level. She has completed six research projects with funding from various agencies, including UGC and DST. She can be contacted at email: krishnaveni_cs@avinuty.ac.in.



Subashini Parthasarathy     is a Professor of the Department of Computer Science, Avinashilingam University for Women in Tamil Nadu, India, since 1994. She is the coordinator of the Centre for machine learning and intelligence, sanctioned by the Department of Science and Technology. She has authored and co-authored 7 books, 9 book chapters, 1 monograph, 194 research papers both at international and national level. She received 15 sponsored research projects worth more than 5.12 crores from various government funding agencies and fostered international collaborations with universities in the USA, Germany, and Morocco. She can be contacted at email: subashini_cs@avinuty.ac.in.